

# Influence of type IV pilus retraction on the architecture of the *Neisseria gonorrhoeae*-infected cell cortex

Dustin L. Higashi,<sup>1†</sup> Gina H. Zhang,<sup>2</sup> Nicolas Biais,<sup>3</sup> Lauren R. Myers,<sup>1</sup> Nathan J. Weyand,<sup>1</sup> David A. Elliott<sup>2</sup> and Magdalene So<sup>1</sup>

## Correspondence

Dustin L. Higashi  
higashid@email.arizona.edu

<sup>1</sup>Department of Immunobiology and the BIO5 Institute, University of Arizona, Tucson, AZ, USA

<sup>2</sup>Department of Cell Biology and Anatomy, College of Medicine, University of Arizona, Tucson, AZ, USA

<sup>3</sup>Department of Biological Sciences, Columbia University, New York, USA

Early in infection, *Neisseria gonorrhoeae* can be observed to attach to the epithelial cell surface as microcolonies and induce dramatic changes to the host cell cortex. We tested the hypothesis that type IV pili (Tfp) retraction plays a role in the ultrastructure of both the host cell cortex and the bacterial microcolony. Using serial ultrathin sectioning, transmission electron microscopy and 3D reconstruction of serial 2D images, we have obtained what we believe to be the first 3D reconstructions of the *N. gonorrhoeae*-host cell interface, and determined the architecture of infected cell microvilli as well as the attached microcolony. Tfp connect both wild-type (wt) and Tfp retraction-deficient bacteria with each other, and with the host cell membrane. Tfp fibres and microvilli form a lattice in the wt microcolony and at its periphery. Wt microcolonies induce microvilli formation and increases of surface area, leading to an approximately ninefold increase in the surface area of the host cell membrane at the site of attachment. In contrast, Tfp retraction-deficient microcolonies do not affect these parameters. Wt microcolonies had a symmetrical, dome-shaped structure with a circular 'footprint', while Tfp retraction-deficient microcolonies were notably less symmetrical. These findings support a major role for Tfp retraction in microvilli and microcolony architecture. They are consistent with the biophysical attributes of Tfp and the effects of Tfp retraction on epithelial cell signalling.

Received 14 July 2009

Revised 27 August 2009

Accepted 15 September 2009

## INTRODUCTION

*Neisseria gonorrhoeae* (the gonococcus, or GC) remains a significant public health concern. The Gram-negative diplococcus causes a million cases of gonorrhoea annually in Western Europe and North America, and over 62 million cases worldwide (World Health Organization). Humans are the only known reservoir for GC. The exquisite tropism of GC for man and the ability of GC to establish a carrier state (Turner *et al.*, 2002) reflect a highly evolved relationship between pathogen and host.

Gonococcal attachment is promoted by type IV pili (Tfp), peritrichous fibres that are 6 nm in width and up to several

micrometres in length. The Tfp filament is composed of helical polymers of pilin subunits (Craig *et al.*, 2006; Parge *et al.*, 1995) and minor proteins (Carbonnelle *et al.*, 2005; Winther-Larsen *et al.*, 2005). Tfp participate in important biological processes such as DNA uptake/genetic exchange, twitching motility, attachment, and host cell signalling (Mattick, 2002; Merz & So, 2000). These activities require, or are enhanced by, the retraction of Tfp fibres (Wolfgang *et al.*, 2000).

Gonococcal Tfp retraction is an activity that requires PilT, the Tfp retraction motor subunit (Wolfgang *et al.*, 1998). Retracting Tfp generate strong 'pull' forces, ranging from ~50 piconewtons (pN) to 1 nanoNewton (nN) (Biais *et al.*, 2008; Merz *et al.*, 2000; Opitz *et al.*, 2009). Repeated cycles of Tfp extension, substrate attachment and Tfp retraction allow GC to crawl over surfaces and aggregate into microcolonies. Tfp retraction from bacteria in a microcolony allows the community to crawl over the epithelial cell surface and fuse with other microcolonies to form larger motile structures (Higashi *et al.*, 2007).

<sup>†</sup>Present address: Department of Immunobiology and the BIO5 Institute, University of Arizona, 1657 E. Helen St, Tucson, AZ 85721, USA.

Abbreviations: GC, gonococcus (*Neisseria gonorrhoeae*); DAPI, 4',6-diamidino-2-phenylindole; Tfp, type IV pili; SEM, scanning electron microscopy; TEM, transmission electron microscopy; wt, wild-type.

Six supplementary movie files are available with the online version of this paper.

Tfp retraction affects the infected epithelial cell at multiple levels. Retraction forces regulate epithelial gene expression and activate cytoprotective signalling pathways (Howie *et al.*, 2005, 2008; Lee *et al.*, 2005). Tfp retraction recruits host cell components to the cortex beneath adhered microcolonies. These cortical plaques are enriched in cytoskeletal and signalling proteins (Edwards *et al.*, 2000; Lee *et al.*, 2005; Merz *et al.*, 1999; Weyand *et al.*, 2006), some of which have been shown to play a role in invasion (Lee *et al.*, 2005; Shaw & Falkow, 1988). The relationship between the cortical plaque and the microcolony is dynamic. As the microcolony crawls over the cell surface, the cortical plaque migrates with it (Higashi *et al.*, 2007). The microcolony–host cell interface is therefore an important focus of study.

A number of microscopy studies have provided important information on the ultrastructure of the infected host cell surface (Edwards *et al.*, 2000; Evans, 1977; Griffiss *et al.*, 1999; McGee *et al.*, 1981; Mosleh *et al.*, 1997; Stephens, 1989; Tjia *et al.*, 1988; Ward *et al.*, 1974). Microvilli are numerous at sites of infection, and they appear to be elongated and deformed. These studies relied on 2D images and selected thin sections of infected cells. Here, we employed serial thin-sectioning, transmission electron microscopy (TEM) and 3D image reconstruction to examine the ultrastructure of a GC infection. We tested the hypothesis that Tfp retraction plays a role in the architecture of the epithelial cell cortex and the infecting microcolonies. We present evidence that wild-type (wt) microcolonies increase the number and surface area of microvilli at sites of infection, leading to a substantial increase in the surface area of the host cell membrane at sites of attachment. In contrast, Tfp retraction-deficient mutants are unable to do so. Wt microcolonies have a symmetrical, spherical shape, while Tfp retraction-deficient mutants have a disordered structure. We discuss these ultrastructural changes in the context of Tfp biodynamics and eukaryotic cell signalling.

## METHODS

**Cell lines and bacterial strains.** The A431 human epidermoid carcinoma cell line (a kind gift of S. Schmid) was used for these studies. These cells have been used previously for neisseria infection studies and their maintenance has been described (Larson *et al.*, 2002; Merz *et al.*, 1999). Briefly, cells were maintained in Dulbecco's Modified Eagle's Medium (DMEM; Mediatech) supplemented with 10 % heat-inactivated fetal bovine serum (FBS; Gibco), and incubated at 37 °C, 5 % CO<sub>2</sub>. Bacterial strains were derivatives of *N. gonorrhoeae* strain MS11 (P+, Opa-non-expressing) (Segal *et al.*, 1986). MS11*pilT* had a null mutation in *pilT*. It produced non-retractable Tfp and was non-motile (Merz *et al.*, 2000; Wolfgang *et al.*, 1998). MS11*pilE* (clone 307) was a non-piliated ( $\Delta$ *pilE1*,  $\Delta$ *pilE2*) strain of MS11 (Ayala *et al.*, 2001; Merz *et al.*, 1996). Bacteria were grown on GCB agar (Difco) with Kellogg's supplements I and II, and maintained at 37 °C, 5 % CO<sub>2</sub>. PilT expression, piliation and Opa status of all strains were monitored by light microscopy of colony morphology, immunoblotting with polyclonal antibodies against PilT (gift of K. T. Forest), and

mAbs against pilin (Merz & So, 1997) and Opa (Achtman *et al.*, 1988).

**Scanning electron microscopy (SEM).** A431 cells were grown to 95 % confluency on Aclar film (Ted Pella, Inc.) in 35 mm dishes and mock-infected with medium or infected with MS11, MS11*pilT* or MS11*pilE* at an m.o.i. of 20 for 3 h. Cells were washed gently in DMEM and fixed in PBS containing glutaraldehyde (2.5 %, w/v) for 1 h at room temperature. Samples were prepared as previously described (Biais *et al.*, 2008). Briefly, cultures were gently washed two times in PBS and dehydrated by successive immersions in ethanol: 50, 70, 80, 90 and 95 % (v/v, in water), and 100 %. Samples were then immersed in three successive baths of 100 % ethanol. Samples were critical point-dried and sputter-coated with platinum. Imaging was done on a Hitachi S-4800 scanning electron microscope.

**Fluorescence microscopy and morphometrics of GC microcolonies.** A431 cells were grown to 70–80 % confluence on coverslips and infected with MS11 or MS11*pilT* at an m.o.i. of 20 for 3 h. The coverslips were then washed three times with PBS, fixed in formaldehyde (3.7 %, w/v, in PBS) for 20 min at room temperature, and incubated with the DNA stain 4',6-diamidino-2-phenylindole (DAPI; diluted 1:1000 in PBS) for 10 min to visualize bacteria. Samples were rinsed extensively with PBS before mounting in Fluoromount-G (Southern Biotech). Samples were imaged using a Nikon Eclipse Ti Microscope using a  $\times$  40 oil objective. In total, 26 wt MS11 and 30 MS11*pilT* microcolonies were analysed for circularity; for each strain, two different images were analysed. The circularity of each microcolony was determined using NIS-Elements AR version 3.0 (Nikon). A perfect circle was assigned a score of 1, while a random shape was assigned a score of 0. Statistical analysis was done using Student's *t* test.

**Serial thin-sectioning and TEM.** A431 cells were grown to 95 % confluency on Aclar film (Ted Pella, Inc.) in 35 mm dishes and mock-infected with medium or infected with MS11 or MS11*pilT* at an m.o.i. of 20 for 3 or 18 h. Cells were washed gently in DMEM and fixed in PBS containing glutaraldehyde (2.5 %, w/v) for 1 h at room temperature. Samples were prepared as previously described (Biais *et al.*, 2008). Briefly, samples were washed three times in PBS and immersed in 1 % osmium tetroxide (1 %, w/v, in PBS, Electron Microscopy Sciences) for 1 h followed by three washes in PBS and a final wash in water. Samples were next incubated for 15 min in 1 % tannic acid (w/v) in water, followed by a wash in water. Samples were then stained with 1 % (w/v) uranyl acetate in water for 1 h. Samples were dehydrated by successive incubations in ethanol: 50, 70 and 90 % (v/v, in water), and 100 % (three successive baths). Infiltration of 50 % embedding Epon (Electron Microscopy Sciences) in ethanol was carried out overnight. Two changes of 1.3 % (v/v) DMP-30 (Ladd Research) in Epon were followed by overnight incubation at 60 °C. Samples were glued onto a chuck, cut into 70 nm serial sections (Elliott, 2007), and prepared as previously described (Elliott *et al.*, 2008). Serial sections were imaged on a Phillips CM-12S transmission electron microscope.

**Quantitation of microvilli and calculation of microvillus geometry.** To quantify microvilli, plasma membrane surface distances were determined by the resolution and magnification (determined pixel size) of random sections from each sample. Microvilli quantification in infected cells was limited to the plasma membrane area under microcolonies along with a 500 nm region flanking the distal-most portion of the colony. Microvilli counts were determined for microvilli that shared a contiguous membrane with the plasma membrane surface in the image. For 3D analysis, digital images were acquired for two independent serial sections of each sample. Images were aligned using AutoAligner 2.0 (Bitplane AG). Video reconstruction and manipulation were done using QuickTime

Pro (Apple). Photoshop CS3 was used to identify microvilli structures and to label them as appropriate. Images were segmented and loaded into Volocity 3.1 (Improvision) for analysis of microvilli geometries and to create 3D models. Pixels had a known volume, as determined from the resolution and magnification of the image, as well as the thickness of each TEM section. Volocity considers all pixels within a villus structure and factors in pixel volume to calculate surface area values. In addition to surface area, skeletal length (defined as the maximum length in the object as determined by eroding evenly from an object's borders inward until only a one-voxel skeleton remains) was measured. Skeletal diameter was defined as the average diameter of an object along the measured skeletal length. Numerical data were exported to Prism 5 (GraphPad Software) for generation of graphs and statistical analyses. Deviations are given as SEM. Statistical analysis was performed using the standard Student's *t* test.

## RESULTS

### SEM of the GC-infected cell cortex

Microvilli beneath GC microcolonies are numerous and appear elongated (Evans, 1977; Griffiss *et al.*, 1999; McGee *et al.*, 1981; Mosleh *et al.*, 1997; Stephens, 1989; Tjia *et al.*, 1988; Ward *et al.*, 1974). We examined GC-infected cells by SEM to determine the role of Tfp in microvillus architecture. A431 human endocervical epithelial cells were mock-infected with medium or infected for 3 h with wt MS11, MS11*pilT* (an isogenic mutant that expresses non-retractable Tfp) or MS11*pilE* (an isogenic mutant that does not produce Tfp). Three independent experiments yielded the same results; images from one experiment are shown in Fig. 1. Mock-infected cells had a few short microvilli (Fig. 1a, i). In contrast, many elongated microvilli were observed at the periphery of wt microcolonies (Fig. 1a, ii). 'Hyper-elongated' microvilli were often observed reaching the apex of wt microcolonies (Fig. 1a, iii). MS11*pilE*, a non-piliated isogenic mutant of MS11, adheres to epithelial cells at a much lower frequency than Tfp-expressing GC (Merz *et al.*, 1996). Of those MS11*pilE* that adhered, few microvilli were observed associated with them (Fig. 1a, iv). Microvilli were also observed at the periphery of *pilT* microcolonies (Fig. 1a, v); however, these were also short compared to the ones associated with wt microcolonies.

Wt and *pilT* microcolonies were always covered with fine filaments. These filaments correlated with Tfp production, as they were not produced by MS11*pilE* (Fig. 1a, iv, b, iii). In wt MS11-infected cells, some Tfp filaments could be seen interconnecting bacteria within the microcolony and making contact with the epithelial cell microvilli (Fig. 1b, i, ii). The interconnective nature of Tfp was consistent with observations using immunofluorescence microscopy (data not shown).

### Morphometrics of GC microcolonies

Wt GC microcolonies appeared to be spherical, while *pilT* microcolonies appeared less ordered (Fig. 1a). The wt shape is consistent with the dynamics of microcolony fusion events. In this process, two or more fusing

microcolonies rapidly become a single sphere through the reorientation of gonococci within the structures (Higashi *et al.*, 2007). We determined whether *pilT* affects microcolony structure by analysing the circularity of their footprints. A431 cells were infected with wt MS11 or MS11*pilT* for 3 h, then stained with DAPI to visualize bacteria by fluorescence microscopy. Two independent experiments yielded similar results. In all, 26 wt and 30 *pilT* microcolonies were analysed for the circularity of their footprints using the NIS-Elements AR program version 3.0 (Nikon). A perfect circle was assigned a score of 1, and a random shape a score of 0. Wt microcolonies had a score of 0.415 ( $\pm 0.021$ ), while *pilT* microcolonies had a score of 0.311 ( $\pm 0.026$ );  $P < 0.004$ , Student's *t* test. Thus, Tfp retraction influences microcolony morphology.

### 3D TEM analysis of the surfaces of GC-infected cells

We further probed GC–microvilli interactions using the technique of serial ultrathin sectioning, TEM, and 3D image reconstruction (Elliott *et al.*, 2008). A431 epithelial cells were infected and processed as described above. Serial 70 nm cross-sections of each sample were cut, stained and imaged by TEM. Over 40 sections were obtained for each microcolony. Images from successive sections were aligned and assembled (see Supplementary Videos S1–S3). Three sequential images from each infection condition are shown in Fig. 2. Two independent experiments yielded similar results.

Consistent with the SEM results, short microvilli were intermittently observed on mock-infected cells (arrowhead, Fig. 2a, Supplementary Video S1), and elongated microvilli were consistently found in close association with wt microcolonies (arrowhead, Fig. 2b, Supplementary Video S2). Tfp fibres were seen connecting wt bacteria within the microcolony. Tfp could also be seen tethered to the epithelial cell membranes (Fig. 2b, right panel). Elongated microvilli were seldom observed in association with *pilT* microcolonies (arrowhead, Fig. 2c). Furthermore, the weaving of microvilli between bacterial cells so characteristic of wt microcolonies was much reduced in *pilT* microcolonies (Fig. 2c, Supplementary Video S3). Tfp fibres were also observed connecting *pilT* bacteria with each other, and between bacteria and the host membrane (Fig. 2c, right panel). SEM and 3D TEM provide independent evidence that Tfp retraction plays a role in inducing microvilli formation and elongation.

### Quantification of microvillus architecture of GC-infected cells by TEM

We first determined the number of microvilli associated with GC microcolonies to establish whether retraction plays a role in microvilli formation. A431 cells were infected for 3 h with wt MS11 or MS11*pilT*, or mock-

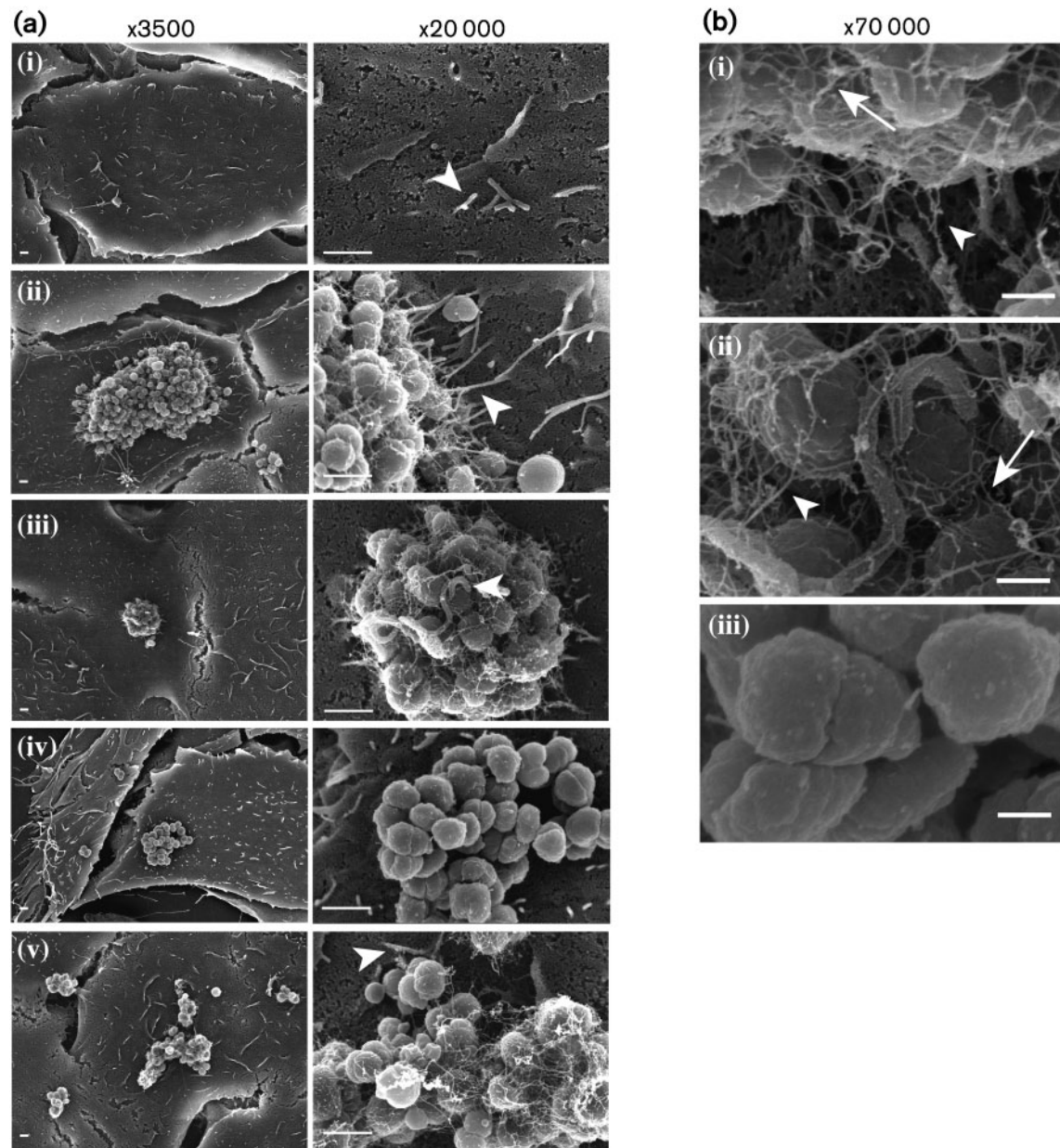


**Fig. 1.** SEM imaging of human epithelial cells infected with *N. gonorrhoeae*. (a) A431 cells were mock-infected with medium (i), or infected with wt MS11 (ii and iii), MS11 *pilE* (iv) or MS11 *pilT* (v) for 3 h. In each row, images in the two magnifications are from the same field of view. Arrowheads highlight microvilli shape/architecture as described in the text. Bars, 1 μm. (b) Enlarged images of wt MS11 (i and ii) and MS11 *pilE* (iii) infected cells from (a). White arrows indicate Tfp connecting bacteria with each other. White arrowheads point to Tfp connecting bacteria to microvilli. Bars, 250 nm.

infected with medium, and the cultures were prepared for thin-sectioning and TEM. Ten random fields from each infection condition were scored for the number of microvilli per unit length (μm) of plasma membrane surface (see Methods). Two independent experiments yielded similar results; one experiment is presented in Fig. 3(a). Mock-infected cells averaged 0.30 (±0.05) microvilli per micrometre of membrane. *pilT* microcolonies had a similar number of microvilli: 0.38 (±0.04,

$P > 0.24$ ) per micrometre of membrane. In contrast, wt microcolonies averaged 1.05 (±0.06,  $P < 0.0001$ ) microvilli per micrometre of membrane. Thus, microvilli are significantly more abundant within wt microcolonies than within *pilT* microcolonies.

We also scored the length, width and membrane surface area of microvilli associated with microcolonies. A431 cells were infected and prepared for thin-sectioning and TEM as

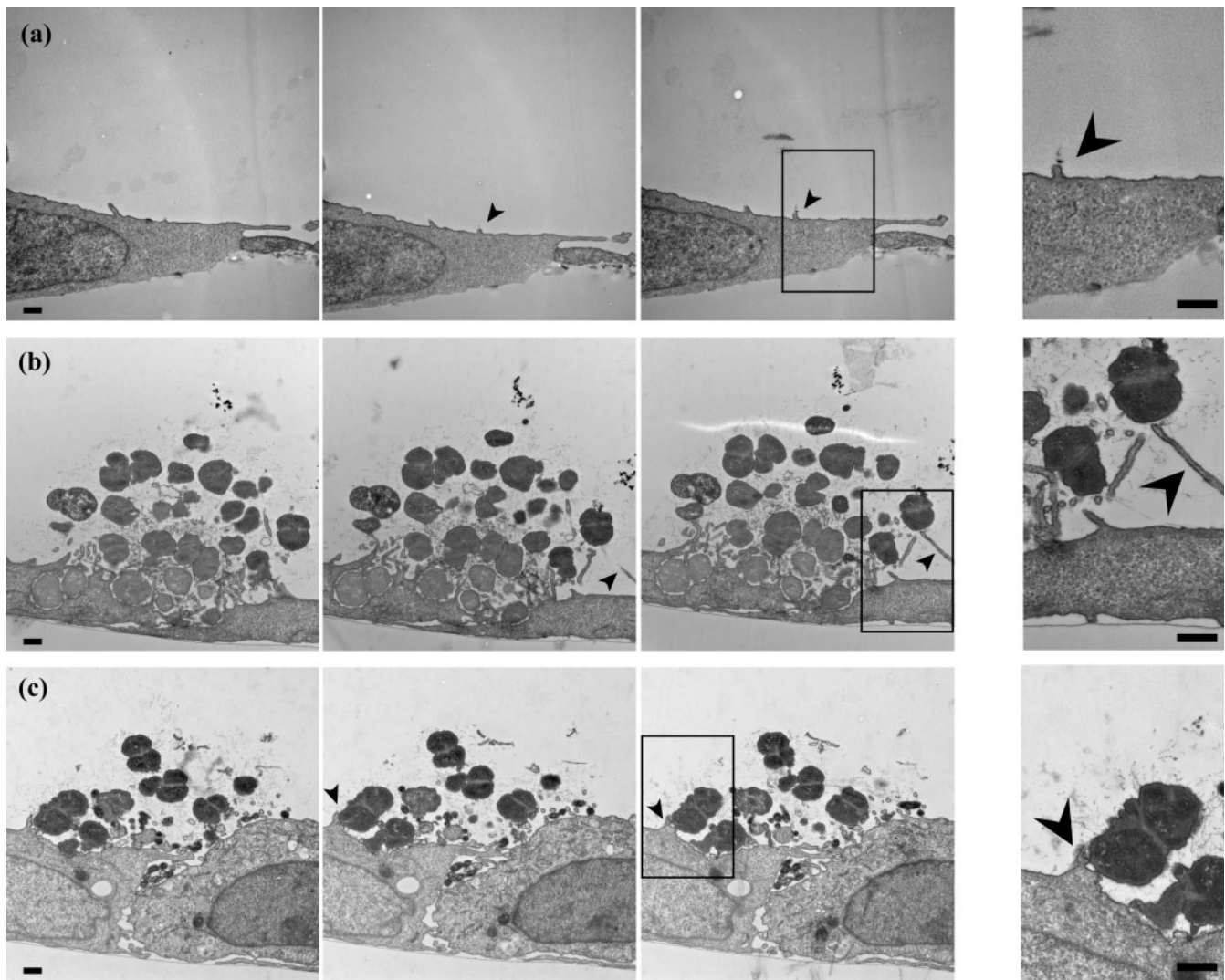


**Fig. 2.** Serial thin-section imaging by TEM of *N. gonorrhoeae*-infected epithelial cells. A431 cells were mock-infected with medium (a), or infected with wt MS11 (b) or MS11 *pilT* (c) for 3 h. Successive serial thin-section (70 nm) images from each sample are shown from left to right. Arrowheads highlight short microvilli in uninfected and *pilT*-infected samples, and elongated microvilli of wt-infected samples. The rightmost panels in each row are enlarged images from the boxed region in the adjacent image. Bars, 500 nm.

described above and in Methods. Two independent experiments yielded similar results; one experiment is shown in Fig. 3(b–d). The surface area of microvilli of mock-infected and *pilT*-infected cells was similar:  $0.42 \mu\text{m}^2$  ( $\pm 0.05$ ) and  $0.36 \mu\text{m}^2$  ( $\pm 0.07$ ), respectively (Fig. 3b). In contrast, the surface area of microvilli of wt-infected cells was  $1.28 \mu\text{m}^2$  ( $\pm 0.15$ ), a threefold increase over the *pilT*- and mock-infected values. The microvilli length of mock-infected cells was  $0.60 \mu\text{m}$  ( $\pm 0.10$ ), and that of *pilT*-infected cells was  $1.00 \mu\text{m}$  ( $\pm 0.34$ ), a modest 1.7-fold increase over the mock-infected value (Fig. 3c). In contrast, the microvilli length of wt-infected cells was  $2.25 \mu\text{m}$  ( $\pm 0.20$ ), a greater than twofold increase over the *pilT*-infected value. There was little difference in the skeletal

diameter of microvilli between mock-, *pilT*- or wt-infected cells:  $0.14 \mu\text{m}$  ( $\pm 0.01$ ),  $0.10 \mu\text{m}$  ( $\pm 0.02$ ) and  $0.13 \mu\text{m}$  ( $\pm 0.01$ ), respectively (Fig. 3d). These results strongly suggest that (1) GC trigger microvilli formation in a *pilT*-dependent manner, and (2) GC trigger microvilli elongation in both a *pilT*-dependent and -independent manner. Animations of representative 3D reconstructions from serial sections of wt (Supplementary Video S4) and *pilT*-infected (Supplementary Video S5) cells illustrate the retraction-dependent changes in the host cell microvillus. Taking into account microvilli number and surface area, we calculate that wt infection leads to an approximately ninefold increase in the total membrane surface area at the infection site.

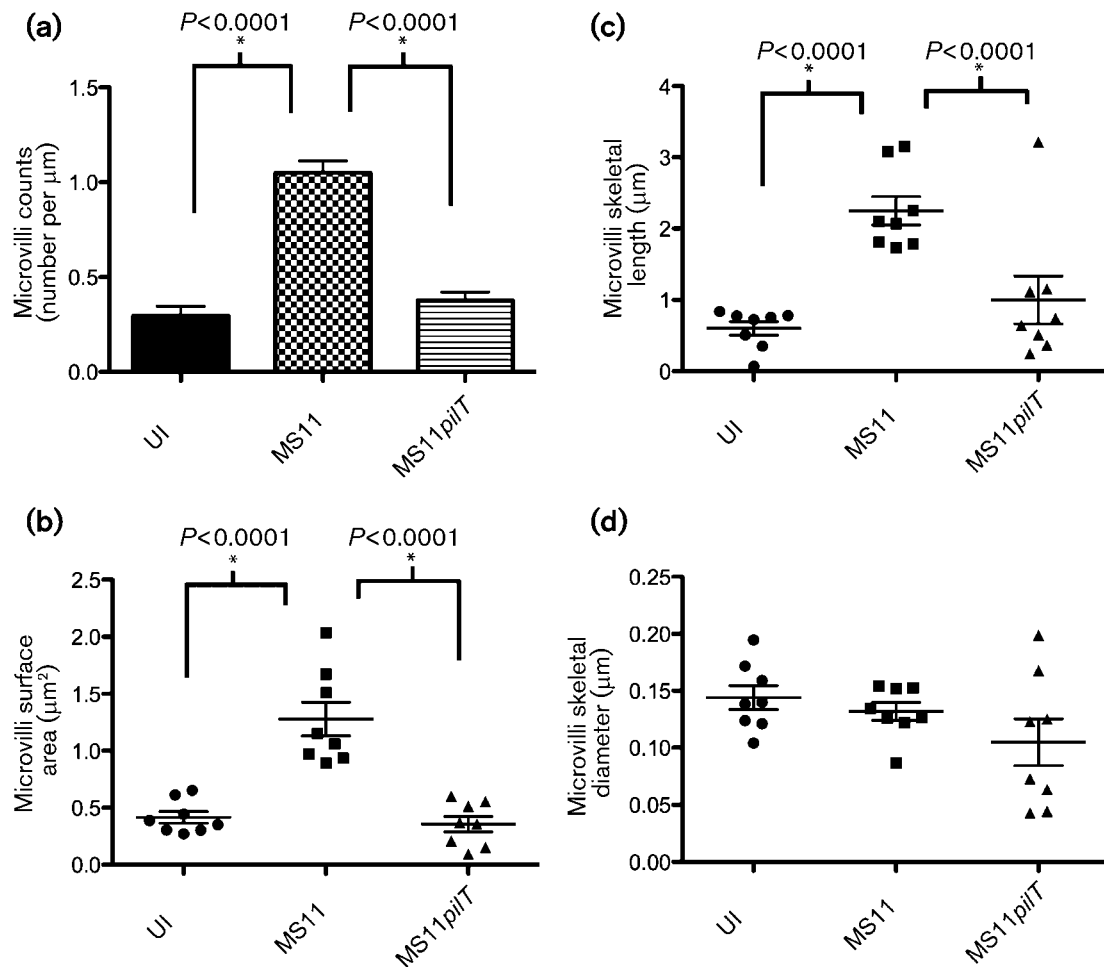


**Fig. 3.** Quantification of microvillus architecture of *N. gonorrhoeae*-infected cells. A431 cells were mock-infected with medium (UI) or infected with wt MS11 or MS11pilT for 3 h, then prepared for TEM. Random fields from each infection condition were scored for various microvilli parameters (see Methods). (a) Microvilli counts were determined by scoring 10 thin-section (70 nm) images of each sample. Values are expressed as the number of microvilli per micrometre of plasma membrane. Values are means from the 10 images with error bars representing SEM. Scatter plots of (b) microvilli surface area, (c) microvilli skeletal length and (d) microvilli skeletal diameter were calculated for each infection condition from two independent 3D datasets. Successive thin-section images of each sample set were scored for each of these attributes as described in Methods. Mean values in each scatter plot are represented by the wide horizontal bars; SEM values are indicated by the error bars.  $P$  values of paired samples are shown (asterisks).

### 3D serial sectioning to probe the intracellularly of GC

Several thin-section images of 3 h infected A431 cells revealed bacteria completely surrounded by host cell membranes, suggesting that these bacteria were intracellular (Fig. 4a, left panel). This contradicted findings from gentamicin protection assays (Shaw & Falkow, 1988), which are commonly used as a measure of intracellular GC. According to this assay, P+, Opa-non-expressing MS11 do not invade cells until 4–5 h post-infection (Hopper *et al.*, 2000; Lin *et al.*, 1997). This quandary was solved when we examined the entire series of thin sections from the same block. The compiled images revealed GC to be enclosed by

the cell at the proximal end (Fig. 4a, left panels) and exposed to the extracellular space at the other (Fig. 4a, right panels). In comparison, 18 h infected cells contained numerous bacteria that were entirely enclosed by host cell membranes (Fig. 4b, Supplementary Video S6). These findings illustrate that random imaging of small numbers of thin sections of infected cells may not be an accurate gauge of the intracellular location of bacteria.

### DISCUSSION

A number of microscopy studies have explored the ultrastructure of the *N. gonorrhoeae*-infected epithelial cell

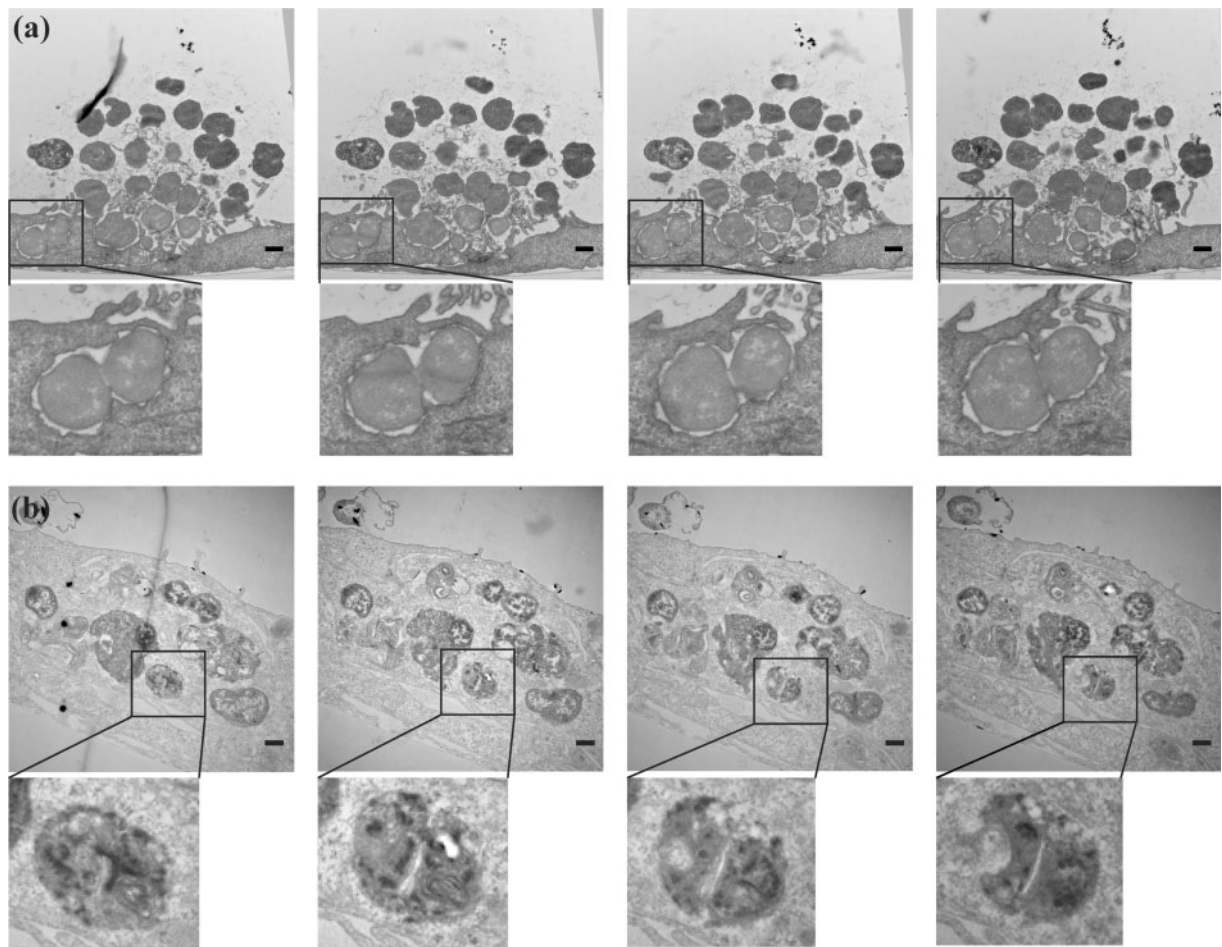


**Fig. 4.** Serial thin-section imaging by TEM of extracellular and intracellular *N. gonorrhoeae*. A431 cells were infected with wt MS11 for 3 h (a) or 18 h (b). Successive serial thin-section (70 nm) images from each sample set are shown from left to right. Boxed regions in each image are enlarged below. Bars, 500 nm.

cortex and the bacterial microcolony (Edwards *et al.*, 2000; Evans, 1977; McGee *et al.*, 1983; Steichen *et al.*, 2008; Stephens, 1989; Swanson, 1983; Ward & Watt, 1972). GC are often seen to attach as microcolonies and to induce dramatic alterations to host cell microvilli, particularly at the microcolony periphery. Here, we used ultrathin sectioning, TEM, and 3D image reconstruction to test the hypothesis that Tfp retraction plays a role in determining the architecture of host cell microvilli and the attached microcolony. We have provided what are believed to be the first 3D ultrastructural reconstructions of the interface between the GC and epithelial cells at an early stage of infection. This interface comprises a structurally ordered community of bacteria interwoven with numerous Tfp and microvilli (Fig. 1). This complex topology of microvilli is seen associated with wt microcolonies, but not *pilT* microcolonies or on mock-infected cells. Microvilli are more numerous under wt microcolonies than under *pilT* microcolonies (Fig. 3a). They are also longer (Fig. 3c) and have a larger surface area (Fig. 3b). The increase in

microvilli number, length and surface area translates to an approximately ninefold increase in total membrane surface area at the GC infection site. These findings strongly suggest that Tfp retraction is an important determinant of microvillus architecture.

How can Tfp retraction alter the shape of the host cell cortex? Artificial forces applied to eukaryotic cell membranes can alter cell architecture and function. Forces as low as 34 pN can induce a lengthening of microvilli (Shao *et al.*, 1998). Slightly higher forces will induce actin-dependent membrane protrusions (Vonna *et al.*, 2003) and activate signalling cascades, calcium fluctuations and tyrosine phosphorylation of numerous proteins (Holm *et al.*, 1999; Sawada *et al.*, 2006; Schmidt *et al.*, 1998). These forces are within the range measured for Tfp retraction (50 pN to 1 nN; Biais *et al.*, 2008; Opitz *et al.*, 2009). Tfp retraction recruits cytoskeletal proteins F-actin and ezrin and signalling proteins to the cell cortex beneath microcolonies (Lee *et al.*, 2005; Merz & So, 1997; Weyand *et al.*,

2006). It also recruits the second lipid messenger phosphatidylinositol (3,4,5)-triphosphate (PIP3) (Lee *et al.*, 2005). Interestingly, the precursor to PIP3, phosphatidylinositol (4,5)-bisphosphate (PIP2), plays a key role in cytoskeletal–membrane adhesion (Raucher *et al.*, 2000). Tfp retraction also induces calcium fluxes in the infected cell (Ayala *et al.*, 2005) and tyrosine phosphorylation of numerous proteins, including PI-3K/Akt (Lee *et al.*, 2005).

What are the function(s) of microvilli at the GC infection site? The weaving of numerous microvilli between bacteria in microcolonies may maximize bacterial exposure to host receptors. It may concentrate receptors and enhance their coupling to ligands. It may serve to restrict signalling pathways to the infection site. Localization of signalling cascades to the site of stimulation is a hallmark of development and neuropeptide signalling. The increased membrane surface area may also provide a corrugated surface that optimizes bacterial attachment (Mikaty *et al.*, 2009). Finally, the additional microvilli may provide the membrane for the bacterial phagosome that will subsequently form (Andrade & Andrews, 2004).

Many other pathogens, such as enterohaemorrhagic *Escherichia coli* (Goosney *et al.*, 2001), *Helicobacter pylori* (Blom *et al.*, 2000; Kwok *et al.*, 2002), *Trypanosoma cruzi* (Andrade & Andrews, 2004) and *Cryptosporidium parvum* (Elliott & Clark, 2000), induce changes to the host plasma membrane and cell cortex during the early stages of infection. These changes are thought to be important in the temporal progression of disease.

Finally, Tfp retraction is a determinant of microcolony structure. How *pilT* influences microcolony morphology is unclear, though previous work strongly suggests that the twitching motility of GC cells within the structure plays a role in influencing its shape. Regardless, the findings in this report identify important issues for the future molecular dissection of gonococcal pathogenesis.

## ACKNOWLEDGEMENTS

We thank Al Agellon (University Spectroscopy and Imaging Facilities; USIF, University of Arizona) for excellent assistance with SEM studies. We thank Dena Yoder (BIO5 Institute) and Chelsea Page for expert technical support. We also thank Shaun Lee and members of the M. So lab for helpful comments on this manuscript. This work was supported in part by NIH grant AI068033 awarded to M. S. and funds from the BIO5 Institute and the College of Medicine, University of Arizona.

## REFERENCES

Achtman, M., Neibert, M., Crowe, B. A., Strittmatter, W., Kusecek, B., Weyse, E., Walsh, M. J., Slawig, B., Morelli, G. & other authors (1988). Purification and characterization of eight class 5 outer membrane protein variants from a clone of *Neisseria meningitidis* serogroup A. *J Exp Med* **168**, 507–525.

Andrade, L. O. & Andrews, N. W. (2004). Lysosomal fusion is essential for the retention of *Trypanosoma cruzi* inside host cells. *J Exp Med* **200**, 1135–1143.

Ayala, B. P., Vasquez, B., Clary, S., Tainer, J. A., Rodland, K. & So, M. (2001). The pilus-induced  $Ca^{2+}$  flux triggers lysosome exocytosis and increases the amount of Lamp1 accessible to *Neisseria* IgA1 protease. *Cell Microbiol* **3**, 265–275.

Ayala, P., Wilbur, J. S., Wetzler, L. M., Tainer, J. A., Snyder, A. & So, M. (2005). The pilus and porin of *Neisseria gonorrhoeae* cooperatively induce  $Ca^{2+}$  transients in infected epithelial cells. *Cell Microbiol* **7**, 1736–1748.

Biais, N., Ladoux, B., Higashi, D., So, M. & Sheetz, M. (2008). Cooperative retraction of bundled type IV pili enables nanonewton force generation. *PLoS Biol* **6**, e87.

Blom, J., Gernow, A., Holck, S., Wewer, V., Norgaard, A., Graff, L. B., Krasinikoff, P. A., Andersen, L. P. & Larsen, S. O. (2000). Different patterns of *Helicobacter pylori* adherence to gastric mucosa cells in children and adults. An ultrastructural study. *Scand J Gastroenterol* **35**, 1033–1040.

Carbannelle, E., Helaine, S., Prouvensier, L., Nassif, X. & Pelicic, V. (2005). Type IV pilus biogenesis in *Neisseria meningitidis*: PilW is involved in a step occurring after pilus assembly, essential for fibre stability and function. *Mol Microbiol* **55**, 54–64.

Craig, L., Volkman, N., Arvai, A. S., Pique, M. E., Yeager, M., Egelman, E. H. & Tainer, J. A. (2006). Type IV pilus structure by cryo-electron microscopy and crystallography: implications for pilus assembly and functions. *Mol Cell* **23**, 651–662.

Edwards, J. L., Shao, J. Q., Ault, K. A. & Apicella, M. A. (2000). *Neisseria gonorrhoeae* elicits membrane ruffling and cytoskeletal rearrangements upon infection of primary human endocervical and ectocervical cells. *Infect Immun* **68**, 5354–5363.

Elliott, D. A. (2007). Serial sectioning via microtomy. *Microscopy Today* **15**, 30–33.

Elliott, D. A. & Clark, D. P. (2000). *Cryptosporidium parvum* induces host cell actin accumulation at the host–parasite interface. *Infect Immun* **68**, 2315–2322.

Elliott, D. A., McIntosh, M. T., Hosgood, H. D., III, Chen, S., Zhang, G., Baevova, P. & Joiner, K. A. (2008). Four distinct pathways of hemoglobin uptake in the malaria parasite *Plasmodium falciparum*. *Proc Natl Acad Sci U S A* **105**, 2463–2468.

Evans, B. A. (1977). Ultrastructural study of cervical gonorrhoea. *J Infect Dis* **136**, 248–255.

Goosney, D. L., DeVinney, R. & Finlay, B. B. (2001). Recruitment of cytoskeletal and signaling proteins to enteropathogenic and enterohemorrhagic *Escherichia coli* pedestals. *Infect Immun* **69**, 3315–3322.

Griffiss, J. M., Lammel, C. J., Wang, J., Dekker, N. P. & Brooks, G. F. (1999). *Neisseria gonorrhoeae* coordinately uses pili and Opa to activate HEC-1-B cell microvilli, which causes engulfment of the gonococci. *Infect Immun* **67**, 3469–3480.

Higashi, D. L., Lee, S. W., Snyder, A., Weyand, N. J., Bakke, A. & So, M. (2007). Dynamics of *Neisseria gonorrhoeae* attachment: microcolony development, cortical plaque formation, and cytoprotection. *Infect Immun* **75**, 4743–4753.

Holm, A., Sundqvist, T., Oberg, A. & Magnusson, K. E. (1999). Mechanical manipulation of polymorphonuclear leukocyte plasma membranes with optical tweezers causes influx of extracellular calcium through membrane channels. *Med Biol Eng Comput* **37**, 410–412.

Hopper, S., Wilbur, J. S., Vasquez, B. L., Larson, J., Clary, S., Mehr, I. J., Seifert, H. S. & So, M. (2000). Isolation of *Neisseria gonorrhoeae* mutants that show enhanced trafficking across polarized T84 epithelial monolayers. *Infect Immun* **68**, 896–905.

Howie, H. L., Glogauer, M. & So, M. (2005). The *N. gonorrhoeae* type IV pilus stimulates mechanosensitive pathways and cytoprotection through a *pilT*-dependent mechanism. *PLoS Biol* **3**, e100.

- Howie, H. L., Shiflett, S. L. & So, M. (2008). Extracellular signal-regulated kinase activation by *Neisseria gonorrhoeae* downregulates epithelial cell proapoptotic proteins Bad and Bim. *Infect Immun* **76**, 2715–2721.
- Kwok, T., Backert, S., Schwarz, H., Berger, J. & Meyer, T. F. (2002). Specific entry of *Helicobacter pylori* into cultured gastric epithelial cells via a zipper-like mechanism. *Infect Immun* **70**, 2108–2120.
- Larson, J. A., Higashi, D. L., Stojiljkovic, I. & So, M. (2002). Replication of *Neisseria meningitidis* within epithelial cells requires TonB-dependent acquisition of host cell iron. *Infect Immun* **70**, 1461–1467.
- Lee, S. W., Higashi, D. L., Snyder, A., Merz, A. J., Potter, L. & So, M. (2005). PilT is required for PI(3,4,5)P3-mediated crosstalk between *Neisseria gonorrhoeae* and epithelial cells. *Cell Microbiol* **7**, 1271–1284.
- Lin, L., Ayala, P., Larson, J., Mulks, M., Fukuda, M., Carlsson, S. R., Enns, C. & So, M. (1997). The *Neisseria* type 2 IgA1 protease cleaves LAMP1 and promotes survival of bacteria within epithelial cells. *Mol Microbiol* **24**, 1083–1094.
- Mattick, J. S. (2002). Type IV pili and twitching motility. *Annu Rev Microbiol* **56**, 289–314.
- McGee, Z. A., Johnson, A. P. & Taylor-Robinson, D. (1981). Pathogenic mechanisms of *Neisseria gonorrhoeae*: observations on damage to human fallopian tubes in organ culture by gonococci of colony type 1 or type 4. *J Infect Dis* **143**, 413–422.
- McGee, Z. A., Stephens, D. S., Hoffman, L. H., Schlech, W. F., III & Horn, R. G. (1983). Mechanisms of mucosal invasion by pathogenic *Neisseria*. *Rev Infect Dis* **5** (suppl. 4), S708–S714.
- Merz, A. J. & So, M. (1997). Attachment of piliated, Opa- and Opc-gonococci and meningococci to epithelial cells elicits cortical actin rearrangements and clustering of tyrosine-phosphorylated proteins. *Infect Immun* **65**, 4341–4349.
- Merz, A. J. & So, M. (2000). Interactions of pathogenic neisseriae with epithelial cell membranes. *Annu Rev Cell Dev Biol* **16**, 423–457.
- Merz, A. J., Rifken, D. B., Arvidson, C. G. & So, M. (1996). Traversal of a polarized epithelium by pathogenic *Neisseriae*: facilitation by type IV pili and maintenance of epithelial barrier function. *Mol Med* **2**, 745–754.
- Merz, A. J., Enns, C. A. & So, M. (1999). Type IV pili of pathogenic neisseriae elicit cortical plaque formation in epithelial cells. *Mol Microbiol* **32**, 1316–1332.
- Merz, A. J., So, M. & Sheetz, M. P. (2000). Pilus retraction powers bacterial twitching motility. *Nature* **407**, 98–102.
- Mikaty, G., Soyer, M., Mairey, E., Henry, N., Dyer, D., Forest, K. T., Morand, P., Guadagnini, S., Prévost, M. C. & other authors (2009). Extracellular bacterial pathogen induces host cell surface reorganization to resist shear stress. *PLoS Pathog* **5**, e1000314.
- Mosleh, I. M., Boxberger, H. J., Sessler, M. J. & Meyer, T. F. (1997). Experimental infection of native human ureteral tissue with *Neisseria gonorrhoeae*: adhesion, invasion, intracellular fate, exocytosis, and passage through a stratified epithelium. *Infect Immun* **65**, 3391–3398.
- Opitz, D., Clausen, M. & Maier, B. (2009). Dynamics of gonococcal type IV pili during infection. *ChemPhysChem* **10**, 1614–1618.
- Parge, H. E., Forest, K. T., Hickey, M. J., Christensen, D. A., Getzoff, E. D. & Tainer, J. A. (1995). Structure of the fibre-forming protein pilin at 2.6 Å resolution. *Nature* **378**, 32–38.
- Raucher, D., Stauffer, T., Chen, W., Shen, K., Guo, S., York, J. D., Sheetz, M. P. & Meyer, T. (2000). Phosphatidylinositol 4,5-bisphosphate functions as a second messenger that regulates cytoskeleton-plasma membrane adhesion. *Cell* **100**, 221–228.
- Sawada, Y., Tamada, M., Dubin-Thaler, B. J., Cherniavskaya, O., Sakai, R., Tanaka, S. & Sheetz, M. P. (2006). Force sensing by mechanical extension of the Src family kinase substrate p130Cas. *Cell* **127**, 1015–1026.
- Schmidt, C., Pommerenke, H., Durr, F., Nebe, B. & Rychly, J. (1998). Mechanical stressing of integrin receptors induces enhanced tyrosine phosphorylation of cytoskeletally anchored proteins. *J Biol Chem* **273**, 5081–5085.
- Segal, E., Hagblom, P., Seifert, H. S. & So, M. (1986). Antigenic variation of gonococcal pilus involves assembly of separated silent gene segments. *Proc Natl Acad Sci U S A* **83**, 2177–2181.
- Shao, J. Y., Ting-Beall, H. P. & Hochmuth, R. M. (1998). Static and dynamic lengths of neutrophil microvilli. *Proc Natl Acad Sci U S A* **95**, 6797–6802.
- Shaw, J. H. & Falkow, S. (1988). Model for invasion of human tissue culture cells by *Neisseria gonorrhoeae*. *Infect Immun* **56**, 1625–1632.
- Steichen, C. T., Shao, J. Q., Ketterer, M. R. & Apicella, M. A. (2008). Gonococcal cervicitis: a role for biofilm in pathogenesis. *J Infect Dis* **198**, 1856–1861.
- Stephens, D. S. (1989). Gonococcal and meningococcal pathogenesis as defined by human cell, cell culture, and organ culture assays. *Clin Microbiol Rev* **2** (suppl.), S104–S111.
- Swanson, J. (1983). Gonococcal adherence: selected topics. *Rev Infect Dis* **5** (suppl. 4), S678–S684.
- Tjia, K. F., van Putten, J. P., Pels, E. & Zanen, H. C. (1988). The interaction between *Neisseria gonorrhoeae* and the human cornea in organ culture. An electron microscopic study. *Graefes Arch Clin Exp Ophthalmol* **226**, 341–345.
- Turner, C. F., Rogers, S. M., Miller, H. G., Miller, W. C., Gribble, J. N., Chromy, J. R., Leone, P. A., Cooley, P. C., Quinn, T. C. & other authors (2002). Untreated gonococcal and chlamydial infection in a probability sample of adults. *JAMA* **287**, 726–733.
- Vonna, L., Wiedemann, A., Aepfelbacher, M. & Sackmann, E. (2003). Local force induced conical protrusions of phagocytic cells. *J Cell Sci* **116**, 785–790.
- Ward, M. E. & Watt, P. J. (1972). Adherence of *Neisseria gonorrhoeae* to urethral mucosal cells: an electron-microscopic study of human gonorrhoea. *J Infect Dis* **126**, 601–605.
- Ward, M. E., Watt, P. J. & Robertson, J. N. (1974). The human fallopian tube: a laboratory model for gonococcal infection. *J Infect Dis* **129**, 650–659.
- Weyand, N. J., Lee, S. W., Higashi, D. L., Cawley, D., Yoshihara, P. & So, M. (2006). Monoclonal antibody detection of CD46 clustering beneath *Neisseria gonorrhoeae* microcolonies. *Infect Immun* **74**, 2428–2435.
- Winther-Larsen, H. C., Wolfgang, M., Dunham, S., van Putten, J. P., Dorward, D., Lovold, C., Aas, F. E. & Koomey, M. (2005). A conserved set of pilin-like molecules controls type IV pilus dynamics and organelle-associated functions in *Neisseria gonorrhoeae*. *Mol Microbiol* **56**, 903–917.
- Wolfgang, M., Lauer, P., Park, H. S., Brossay, L., Hebert, J. & Koomey, M. (1998). PilT mutations lead to simultaneous defects in competence for natural transformation and twitching motility in piliated *Neisseria gonorrhoeae*. *Mol Microbiol* **29**, 321–330.
- Wolfgang, M., van Putten, J. P., Hayes, S. F., Dorward, D. & Koomey, M. (2000). Components and dynamics of fiber formation define a ubiquitous biogenesis pathway for bacterial pili. *EMBO J* **19**, 6408–6418.

Edited by: P. van der Ley